3D simulation of superconducting magnetic shields and lenses using the fast Fourier transform

Leonid Prigozhin[1,a)] and Vladimir Sokolovsky[2,a)]
[1]*J. Blaustein Institutes for Desert Research, Ben-Gurion University of the Negev, Sede Boqer Campus, Midreshet Ben-Gurion 84990, Israel*
[2]*Physics Department, Ben-Gurion University of the Negev, Beer-Sheva 84105, Israel*

(Received 4 March 2018; accepted 18 May 2018; published online 19 June 2018)

Shielding sensitive scientific and medical devices from the magnetic field environment is one of the promising applications of superconductors. Magnetic field concentration by superconducting magnetic lenses is the opposite phenomenon based, however, on the same properties of superconductors: their ideal conductivity and ability to expel the magnetic field. Full-dimensional numerical simulations are necessary for designing magnetic lenses and for estimating the quality of magnetic shielding under arbitrary varying external fields. Using the recently proposed Fast Fourier Transform based three-dimensional numerical method [Prigozhin and Sokolovsky, Supercond. Sci. Technol. **31**, 055018 (2018)], we model performance of two such devices made of a bulk type-II superconductor: a magnetic shield and a magnetic lens. The method is efficient and can be easier to implement than the alternative approaches based on the finite element methods. *Published by AIP Publishing*. https://doi.org/10.1063/1.5027592

I. INTRODUCTION

Superconductor and hybrid superconductor/ferromagnet systems are able to efficiently shield stronger magnetic fields than the purely ferromagnet systems and to provide large magnetic field attenuations; see Refs. 1–4 and the references therein. Hollow superconductor cylinders, either open or closed at one end, are often employed to shield the area inside their hole. The efficiency of shielding has usually been estimated for a uniform external field either parallel to the cylinder axis[1–3] or perpendicular to it.[1] Since in the latter case the cylinder was assumed infinitely long, both configurations were described by two-dimensional models. The problem of shielding a non-uniform axisymmetric field could also be reduced to a two-dimensional one.[5] The only solution of a three-dimensional (3D) shielding problem for bulk superconductors we know was obtained in Ref. 4 for a general non-uniform field using the *h*-formulation and the finite element software GetDP. Another finite element package, COMSOL Multiphysics, was employed in Ref. 6 for 3D numerical simulation of shielding by cylinders made of several layers of a coated conductor tape.

For a finite cylinder, the problem is 3D also if the applied field is uniform, but not parallel to the cylinder axis. Here, we solve such a 3D problem for a hollow superconducting cylinder sealed at one end (the configuration considered in Ref. 2) using the Fast Fourier Transform (FFT) based method.[7] This method is an easily implemented alternative to the finite element methods for 3D magnetization problems (see, e.g., Refs. 8–16), and we employ it to model also field concentration by a magnetic lens. The configuration of a bulk superconductor in the latter problem is that of the magnetic lenses in Ref. 17.

We note that an FFT-based numerical method for superconductivity problems was first proposed for thin film magnetization problems in Ref. 18 and then applied to modeling thermal instabilities and flux avalanches in superconducting films; see, e.g., Refs. 19–22. In our work,[7] a new 3D FFT-based method for bulk magnetization problems was derived and compared to the finite element methods by solving two model problems (magnetization of a superconducting cube and a hollow ball). An extension of this method to multiply connected domains was also proposed. As in the 2D thin film case, the 3D method employs FFT for the approximation in space and the method of lines for integration in time. However, the proposed method uses the magnetic field as the main variable and is based on a different problem formulation. For completeness, we briefly describe this method in Sec. II; further details can be found in Ref. 7.

Here, for the first time, we demonstrate applicability of the 3D FFT-based method to realistic magnetization problems arising in practical applications of bulk type-II superconductors. Although we assumed a field-independent isotropic power law current-voltage relation characterizing the superconductor material, our 3D method allows one to use a different relation to account for a critical current density dependence on the magnetic field, anisotropy of a superconductor, or the flux cutting effect in force free configurations. However, the method is currently not applicable to problems with transport current and/or infinitely long cables.

All numerical simulations in this work have been performed in Matlab R2017a on a PC with Intel(R) Core(TM) i5-2400 CPU @ 3.10 GHz, 16 GB RAM, Windows 7 (64-bit). As an example, our programs for the magnetic lens simulation are presented as a supplementary material (can also be downloaded from Ref. 23). Adapting these programs to a different geometry and another current-voltage relation should not be difficult.

[a)]E-mail addresses: leonid@math.bgu.ac.il and sokolovv@bgu.ac.il

II. FFT-BASED METHOD FOR BULK MAGNETIZATION PROBLEMS

Let $\Omega \subset R^3$ be the 3D domain occupied by a superconductor, Γ—its boundary, and $\boldsymbol{j}$—the current density satisfying $\nabla \cdot \boldsymbol{j} = 0$ in Ω and having a zero normal component, $j_n = 0$, on Γ. For simplicity, we assume that the applied external magnetic field $\boldsymbol{h}_e(t)$ is uniform and $\boldsymbol{j} = \boldsymbol{0}$ in the exterior domain $\Omega_{out} = R^3 \backslash (\Omega \cup \Gamma)$. We will restrict our consideration to the contourwise simply connected domains (every closed contour in the domain can be presented as a boundary of a surface also belonging to this domain) and refer to Ref. 7 for a discussion of the more complicated multiply connected case. As is most often done, we assume that the electric field $\boldsymbol{e}$ and the current density $\boldsymbol{j}$ in the superconductor are parallel and

$$\boldsymbol{e} = \rho(|\boldsymbol{j}|)\boldsymbol{j}, \tag{1}$$

where $\rho(|\boldsymbol{j}|) = (e_0/j_c)|\boldsymbol{j}/j_c|^{n-1}$ is the nonlinear resistivity, the power n and the critical current density j_c are constant, and $e_0 = 10^{-4}$ V m^{-1}. A different nonlinear current-voltage relation, $\boldsymbol{e}(\boldsymbol{j})$ or $\boldsymbol{e}(\boldsymbol{j}, \boldsymbol{h})$, where $\boldsymbol{h}$ is the local magnetic field, can also be employed.

By the Biot-Savart law

$$\boldsymbol{h} = \boldsymbol{h}_e + \boldsymbol{\Phi}[\boldsymbol{j}], \tag{2}$$

where $\boldsymbol{\Phi}[\boldsymbol{j}] = \nabla \times \int_\Omega G(\boldsymbol{r} - \boldsymbol{r}')\boldsymbol{j}(\boldsymbol{r}', t)\, d\boldsymbol{r}'$, $G(\boldsymbol{r}) = (4\pi|\boldsymbol{r}|)^{-1}$ is the Green function, and $\boldsymbol{r} = (x, y, z)$. Clearly, by the Ampere law, $\nabla \times \boldsymbol{\Phi}[\boldsymbol{j}] = \nabla \times [\boldsymbol{h} - \boldsymbol{h}_e(t)] = \nabla \times \boldsymbol{h} = \boldsymbol{j}$.

To formulate an evolutionary problem for $\boldsymbol{h}$, we use the Faraday law

$$\mu_0 \dot{\boldsymbol{h}} = -\nabla \times \boldsymbol{e}, \tag{3}$$

where μ_0 is the magnetic permeability of vacuum and the point above a variable means the time derivative. Let at time t the magnetic field $\boldsymbol{h}$ be known. Then

$$\boldsymbol{j} = \nabla \times \boldsymbol{h} \tag{4}$$

and electric field in Ω is determined by (1). However, $\boldsymbol{e}$ remains undetermined in the non-conductive domain Ω_{out}. A possible way to deal with this complication is to replace the non-conducting surrounding by a poor conductor obeying, e.g., the linear Ohm law $\boldsymbol{e} = \rho_{out}\boldsymbol{j}$ with a high resistivity ρ_{out}. Such a solution is not ideal: if ρ_{out} is high, the evolutionary problem is stiff, otherwise a non-negligible current appears in Ω_{out}. In Ref. 7, the Ohm law is used to define, for each t, the electric field in Ω_{out} only on the initial step of an iterative determination of $\dot{\boldsymbol{h}}$. After this step, the values of $\dot{\boldsymbol{h}}$ in Ω remain unchanged, while in Ω_{out} they are modified in the course of iterations ensuring that $\dot{\boldsymbol{j}}_{out} = \nabla \times \dot{\boldsymbol{h}}|_{\Omega_{out}} = \boldsymbol{0}$ and thus no stray current in this domain appears. The role of the fictitious resistivity ρ_{out} is to efficiently suppress the stray current only in a thin boundary layer outside the superconductor; the iterations take care of this current in the rest of Ω_{out}.

We now describe the iterative algorithm in detail. To find $\dot{\boldsymbol{h}}$ at time t we compute $\boldsymbol{j} = \nabla \times \boldsymbol{h}$, set

$$\boldsymbol{e} = \begin{cases} \rho(\boldsymbol{j})\boldsymbol{j} & \text{in } \Omega, \\ \rho_{out}\boldsymbol{j} & \text{in } \Omega_{out}, \end{cases}$$

find $\dot{\boldsymbol{h}}_{in} = -\mu_0^{-1}\nabla \times \boldsymbol{e}|_\Omega$, and define an initial approximation, $\dot{\boldsymbol{h}}^0_{out}$, in Ω_{out}. Then, on the i-th iteration, we compute $\dot{\boldsymbol{j}}^i = \nabla \times \dot{\boldsymbol{h}}^i$ and set

$$\dot{\boldsymbol{h}}^{i+1}_{out} = \dot{\boldsymbol{h}}_e + \boldsymbol{\Phi}\left[\dot{\boldsymbol{j}}^i_{in}\right]|_{\Omega_{out}}, \tag{5}$$

where $\dot{\boldsymbol{j}}^i_{in} = \dot{\boldsymbol{j}}^i$ in Ω and zero in Ω_{out}. Provided these iterations converge, $\nabla \times \dot{\boldsymbol{h}}|_{\Omega_{out}} = (\dot{\boldsymbol{j}}_{in})|_{\Omega_{out}} = \boldsymbol{0}$ as desired.

The operator $\boldsymbol{\Phi}$ can be expressed by means of convolutions in R^3

$$\boldsymbol{\Phi}[\boldsymbol{j}] = \begin{Bmatrix} j_z * \partial_y G - j_y * \partial_z G \\ j_x * \partial_z G - j_z * \partial_x G \\ j_y * \partial_x G - j_x * \partial_y G \end{Bmatrix}. \tag{6}$$

Since the Fourier transform of G in R^3 is $F(G) = \int_{R^3} G(\boldsymbol{r})\, e^{-i\boldsymbol{k}\cdot\boldsymbol{r}} d\boldsymbol{r} = 1/|\boldsymbol{k}|^2$, where $\boldsymbol{k} = (k_x, k_y, k_z)$, see, Refs. 24 and 25, Eq. (6) can be rewritten as

$$\boldsymbol{\Phi}[\boldsymbol{j}] = F^{-1}\left\{ \frac{i}{|\boldsymbol{k}|^2} \begin{bmatrix} k_y F(j_z) - k_z F(j_y) \\ k_z F(j_x) - k_x F(j_z) \\ k_x F(j_y) - k_y F(j_x) \end{bmatrix} \right\}. \tag{7}$$

This expression is not determined for $\boldsymbol{k} = \boldsymbol{0}$ but, taking into account that $\int_{R^3} \boldsymbol{\Phi}[\boldsymbol{j}] d\boldsymbol{r} = \int_{R^3} [\boldsymbol{h} - \boldsymbol{h}_e(t)]\, d\boldsymbol{r}$ should be zero at each moment in time, for $\boldsymbol{k} = \boldsymbol{0}$ we replace $1/|\boldsymbol{k}|^2$ in (7) by zero.

To make this algorithm practical, a uniform $N_x \times N_y \times N_z$ grid should be defined in the computational domain $D = \{ (x, y, z) \mid |x| \le L_x, |y| \le L_y, |z| \le L_z \}$ containing Ω and some empty space around it; the Fourier transform and its inverse should be replaced by their discrete counterparts on this grid and the FFT algorithm employed. As in Ref. 7, we computed the spatial derivatives in (3) and (4) in the Fourier space and applied the Gaussian smoothing; the smoothing parameter σ was equal to a half of the grid cell diagonal. The spatially discretized algorithm provides an approximation to $\dot{\boldsymbol{h}}$ values in the grid nodes for a given set of $\boldsymbol{h}$ node values; the resulting system of ordinary differential

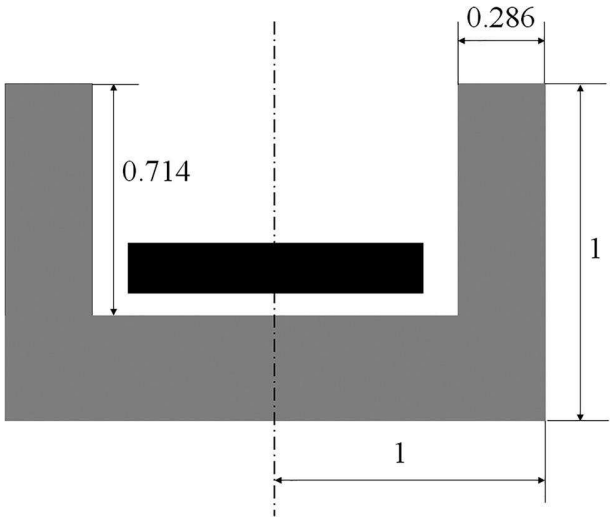

FIG. 1. Scheme of the superconducting shield (gray); dimensionless units. The black area is the shielded zone.

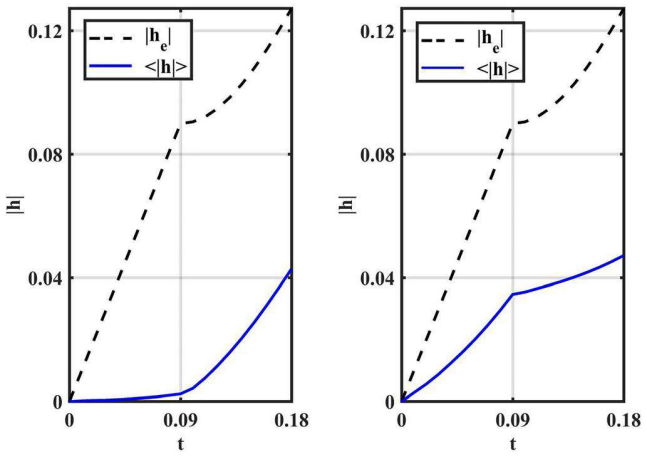

FIG. 2. Shielding performance, different variations of the external field: left—case A, right—case B. Dashed line—the applied field magnitude, solid line—the average magnetic field magnitude in the shielded zone.

equations (ODE) was integrated in time by the standard Matlab ODE solver ode23 (with the relative tolerance 2×10^{-4}). At each time step, the iterations (5) were performed until the average of the node values of $|\dot{\boldsymbol{h}}^{i+1} - \dot{\boldsymbol{h}}^{i}|$ in Ω_{out} becomes less than $\delta_{\text{it}} \max(|\dot{\boldsymbol{h}}_{\text{e}}|, 1)$, where $\delta_{\text{it}} = 2 \times 10^{-5}$ was the prescribed tolerance. As the initial approximation $\dot{\boldsymbol{h}}^{0}_{\text{out}}$, we used $\dot{\boldsymbol{h}}_{\text{out}}$ from the previous time step and, usually, the convergence was achieved in a few iterations.

III. SIMULATION RESULTS

In our simulations, the virgin initial state was assumed and the power $n = 30$. We used dimensionless variables

$$(x', y', z') = \frac{(x, y, z)}{l}, \quad t' = \frac{t}{t_0}, \quad \boldsymbol{e}' = \frac{\boldsymbol{e}}{e_0}, \quad \boldsymbol{j}' = \frac{\boldsymbol{j}}{j_{\text{c}}}, \quad \boldsymbol{h}' = \frac{\boldsymbol{h}}{j_{\text{c}} l}, \tag{8}$$

where l is the characteristic size and $t_0 = \mu_0 j_{\text{c}} l^2 / e_0$; below, the prime is omitted.

Our first example is a hollow, closed at one end superconducting cylinder (Fig. 1); its sizes are taken from Ref. 2 and scaled in accordance with (8). The cylinder was centrally positioned in a cube with sides 3.2 (the computation domain); in this example we set $\rho_{\text{out}} = 20$. We considered two cases. Case A: the external field first grows along the cylinder axis, then in a direction perpendicular to it: $\boldsymbol{h}_{\text{e}} = (0, 0, t)$ for $0 \le t \le \tau$ and $\boldsymbol{h}_{\text{e}} = (t - \tau, 0, \tau)$ for $\tau \le t \le 2\tau$ with $\tau = 0.09$. Case B: same variations in the inverse order, $\boldsymbol{h}_{\text{e}} = (t, 0, 0)$ for $0 \le t \le \tau$ and $\boldsymbol{h}_{\text{e}} = (\tau, 0, t - \tau)$ for

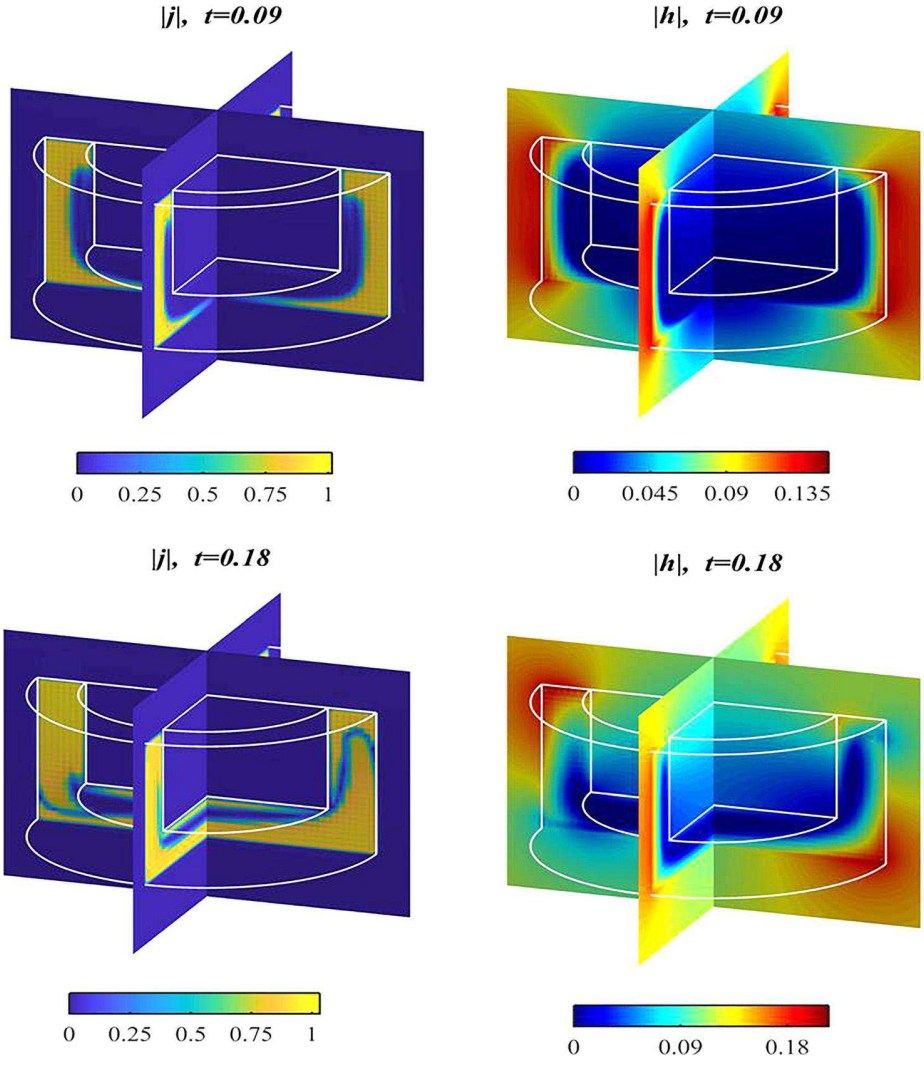

FIG. 3. Magnetic shield simulation (case A). Magnitudes of the current density (left) and magnetic field (right) in the cross-sections $x = 0$ and $y = 0$.

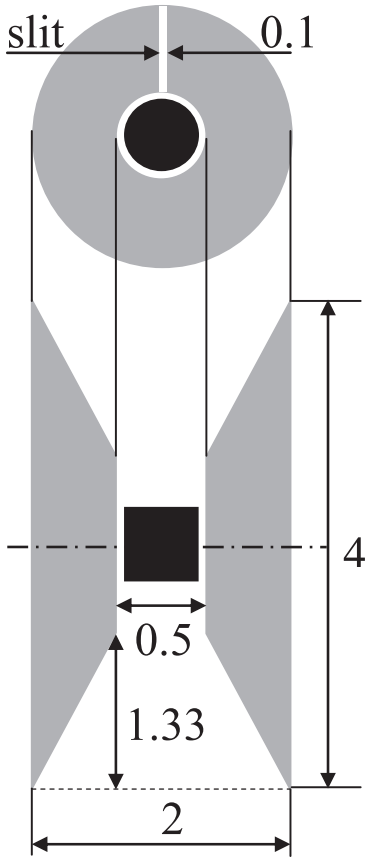

FIG. 4. Scheme of the magnetic superconducting lens (gray) and the lens central region (black).

$\tau \le t \le 2\tau$. To illustrate the shielding performance, we compared the applied field magnitude $|\boldsymbol{h}_e|$ with the mean magnitude $\langle|\boldsymbol{h}|\rangle$ of the magnetic field inside the "shielded zone" defined as a disk, co-axial to the cylinder, having the thickness 0.143, radius 0.667, and the middle plane at 0.452 below the cylinder top (Fig. 1). Because the cylinder is short, fields perpendicular to its axis penetrate the shielded zone much easier than a field parallel to this axis, see Fig. 2. For the $128 \times 128 \times 128$ grid, our computations took about two hours and for the $192 \times 192 \times 192$ grid—twelve hours; the solutions obtained for these grids were close.

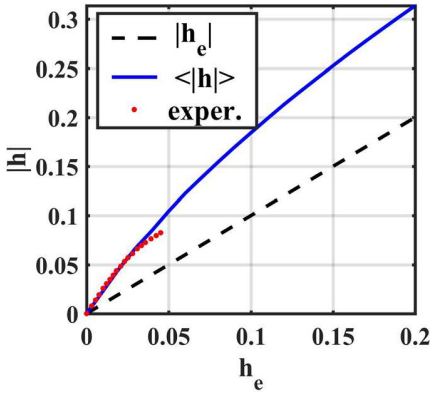

FIG. 5. Magnetic field magnitude in the lens central region: solid line—numerical simulation (averaged), dotted line—measurements.[17] Dashed line—the applied field magnitude.

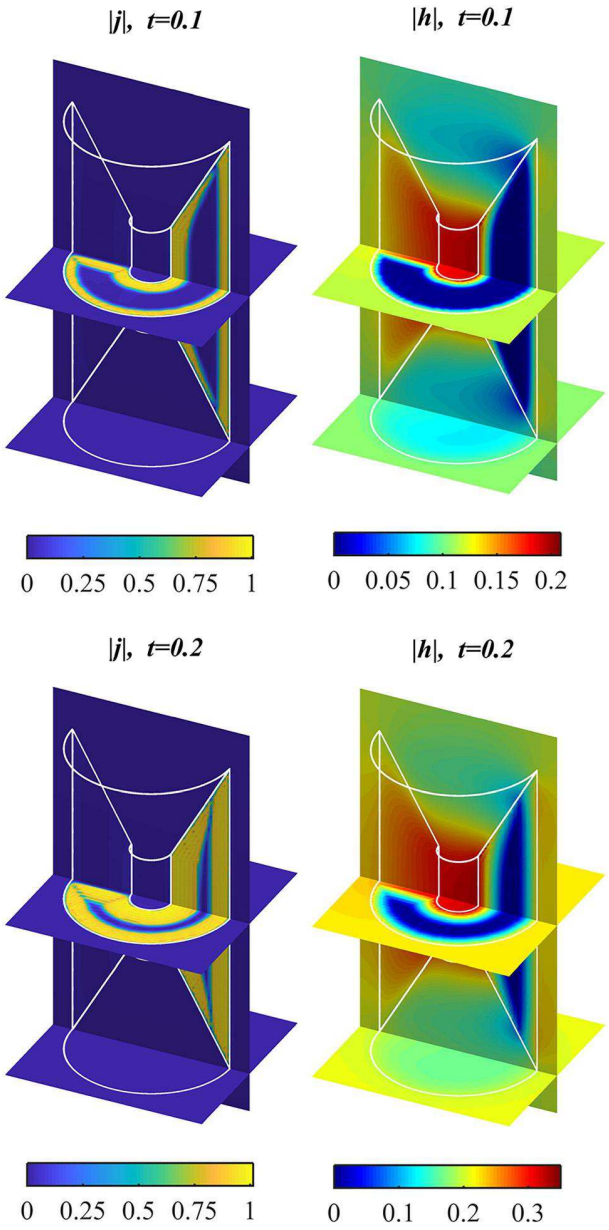

FIG. 6. Superconducting magnetic lens. Magnitudes of the current density (left) and magnetic field (right) in the cross-sections $x = 0$, $z = 0$, and $z = -2$.

In Ref. 2, the magnetic field was applied parallel to the cylinder axis and beginning of the field penetration into the shielded area has been observed at about 0.6 T (see Fig. 2 in Ref. 2) In our simulation (Fig. 2, left), the penetration starts at about 0.08 (dimensionless units) which corresponds to 0.6 T for the critical current density 6×10^8 A/m^2; this is a reasonable value for a bulk MgB_2 superconductor at 20 K.

The calculated distributions of the magnetic field and current density for the case A at $t = \tau$ and $t = 2\tau$ are presented in Fig. 3.

The magnetic lens in our second example (Fig. 4) is geometrically similar to those studied experimentally in Ref. 17: it is a superconducting cylinder with a coaxial biconical hole and

a narrow slit to prevent the shielding circumference current. The applied field was parallel to the cylinder axis, $\boldsymbol{h}_e = (0, 0, t)$, $0 \le t \le 0.2$. In this example, we used a higher value of the fictitious resistivity, $\rho_{out} = 100$, to fully suppress the flow of current through the narrow slit and the $128 \times 128 \times 256$ grid in the computational domain $\{|x| \le 1.8, |y| \le 1.8, |z| \le 3.6\}$. The computation time was about six hours. Partially expelled from the superconductor, magnetic field is concentrated in the central part of the lens. The calculated average field magnitude in the central region $\{r \le 0.2, |z| \le 0.33\}$ is about twice bigger than the applied field for $|\boldsymbol{h}_e| = 0.05$ and 1.6 times bigger for $|\boldsymbol{h}_e| = 0.2$ (Fig. 5). The red dots in this figure show the measured magnitude of magnetic field in the lens center (Ref. 17, Fig. 4, sample A at 20 K) scaled in accordance with (8) with the cylinder outer radius $l = 14.5$ mm and the critical current density at zero field and temperature 20 K, $j_c = 1150\,\mathrm{A/mm^2}$ (Ref. 17, Table 3). Without any fitting or parameter adjustment, our numerical results are in very good agreement with the experimental data. Only as the growing external field becomes close to 1 T (slightly less than 0.05 in dimensionless units), there appears a deviation which can be explained by the dependence of the critical current density on magnetic field (see Ref. 17, Table 3) not taken into account in this simulation. The computed current density and magnetic field distributions are presented in Fig. 6 for $t = 0.1$ and $t = 0.2$.

IV. CONCLUSION

In many cases, design of superconductor devices needs a solution of highly nonlinear 3D electromagnetic problems. Development of numerical methods for these problems is currently an active field of research.

The presented solutions of two problems, shielding and concentration of magnetic field by bulk superconductors, confirm the efficiency of the new 3D FFT-based method[7] and agree well with the available experimental data. These solutions illustrate the ability of the FFT-based method to solve realistic magnetization problems for superconductors of different shapes. The method is simple, easy to implement, and can be used with any current-voltage relation characterizing the superconducting material (iso- or anisotropic, field dependent, etc.).

SUPPLEMENTARY MATERIAL

See supplementary material for our Matlab implementation of the 3D FFT-based method (the magnetic lens simulation example).

[1]J.-F. Fagnard, M. Dirickx, M. Ausloos, G. Lousberg, B. Vanderheyden, and P. Vanderbemden, "Magnetic shielding properties of high-Tc superconducting hollow cylinders: Model combining experimental data for axial and transverse magnetic field configurations," Supercond. Sci. Technol. **22**, 105002 (2009).

[2]L. Gozzelino, R. Gerbaldo, G. Ghigo, F. Laviano, M. Truccato, and A. Agostino, "Superconducting and hybrid systems for magnetic field shielding," Supercond. Sci. Technol. **29**, 034004 (2016).

[3]L. Wéra, J. F. Fagnard, D. K. Namburi, Y. Shi, B. Vanderheyden, and P. Vanderbemden, "Magnetic shielding above 1 T at 20 K with bulk, large grain YBCO tubes made by buffer-aided top seeded melt growth," IEEE Trans. Appl. Supercond. **27**, 1–5 (2017).

[4]K. Hogan, J.-F. Fagnard, L. Wéra, B. Vanderheyden, and P. Vanderbemden, "Bulk superconducting tube subjected to the stray magnetic field of a solenoid," Supercond. Sci. Technol. **31**, 015001 (2018).

[5]K. Hogan, J.-F. Fagnard, L. Wera, B. Vanderheyden, and P. Vanderbemden, "Magnetic shielding of an inhomogeneous magnetic field source by a bulk superconducting tube," Supercond. Sci. Technol. **28**, 035011 (2015).

[6]Y. Nagasaki, M. Solovyov, and F. Gömöry, "Experimental and numerical investigation of shielding performance of superconducting magnetic shields using coated conductor tapes," IEEE Trans. Appl. Supercond. **28**, 1–5 (2018).

[7]L. Prigozhin and V. Sokolovsky, "Fast Fourier transform-based solution of 2D and 3D magnetization problems in type-II superconductivity," Supercond. Sci. Technol. **31**, 055018 (2018).

[8]C. M. Elliott and Y. Kashima, "A finite-element analysis of critical-state models for type-II superconductivity in 3D," IMA J. Numer. Anal. **27**, 293–331 (2007).

[9]Y. Kashima, "On the double critical-state model for type-II superconductivity in 3D," ESAIM: Math. Modell. Numer. Anal. **42**, 333–374 (2008).

[10]M. Zhang and T. Coombs, "3D modeling of high-T_c superconductors by finite element software," Supercond. Sci. Technol. **25**, 015009 (2012).

[11]A. Stenvall, V. Lahtinen, and M. Lyly, "An H-formulation-based three-dimensional hysteresis loss modelling tool in a simulation including time varying applied field and transport current: The fundamental problem and its solution," Supercond. Sci. Technol. **27**, 104004 (2014).

[12]M. Kapolka, J. Srpcic, D. Zhou, M. D. Ainslie, E. Pardo, and A. R. Dennis, "Demagnetization of cubic Gd-Ba-Cu-O Bulk superconductor by crossed-fields: Measurements and three-dimensional modeling," IEEE Trans. Appl. Supercond. **28**, 1–5 (2018).

[13]M. Kapolka, V. M. R. Zermeño, S. Zou, A. Morandi, P. L. Ribani, E. Pardo, and F. Grilli, "Three-dimensional modeling of the magnetization of superconducting rectangular-based bulks and tape stacks," IEEE Trans. Appl. Supercond. **28**, 8201206 (2018).

[14]E. Pardo and M. Kapolka, "3D computation of non-linear eddy currents: Variational method and superconducting cubic bulk," J. Comput. Phys. **344**, 339–363 (2017).

[15]E. Pardo and M. Kapolka, "3D magnetization currents, magnetization loop, and saturation field in superconducting rectangular prisms," Supercond. Sci. Technol. **30**, 064007 (2017).

[16]M. Olm, S. Badia, and A. F. Martín, "Simulation of high temperature superconductors and experimental validation," preprint arXiv:1707.09783 (2017).

[17]Z. Y. Zhang, S. Choi, S. Matsumoto, R. Teranishi, G. Giunchi, A. F. Albisetti, and T. Kiyoshi, "Magnetic lenses using different MgB 2 bulk superconductors," Supercond. Sci. Technol. **25**, 025009 (2012).

[18]J. I. Vestgården and T. H. Johansen, "Modeling non-local electrodynamics in superconducting films: The case of a right angle corner," Supercond. Sci. Technol. **25**, 104001 (2012).

[19]J. Brisbois, O.-A. Adami, J. Avila, M. Motta, W. A. Ortiz, N. D. Nguyen, P. Vanderbemden, B. Vanderheyden, R. B. Kramer, and A. Silhanek, "Magnetic flux penetration in Nb superconducting films with lithographically defined microindentations," Phys. Rev. B **93**, 054521 (2016).

[20]Z. Jing, H. Yong, and Y. Zhou, "Influences of non-uniformities and anisotropies on the flux avalanche behaviors of type-II superconducting films," Supercond. Sci. Technol. **29**, 105001 (2016).

[21]J. I. Vestgården, F. Colauto, A. De Andrade, A. A. M. Oliveira, W. A. Ortiz, and T. H. Johansen, "Cascade dynamics of thermomagnetic avalanches in superconducting films with holes," Phys. Rev. B **92**, 144510 (2015).

[22]J. I. Vestgården, P. Mikheenko, Y. M. Galperin, and T. H. Johansen, "Nonlocal electrodynamics of normal and superconducting films," New J. Phys. **15**, 093001 (2013).

[23]See https://www.cs.bgu.ac.il/~leonid/3D_magn_lens_programs.rar for "3D FFT-Based Method: The Matlab Program (Magnetic Lens Simulation)" (2018).

[24]See https://en.wikipedia.org/wiki/Fourier_transform for "Fourier Transform, Formula 502."

[25]M. Reiher and A. Wolf, "E.2: Fourier transformations of the Coulomb potential," in *Relativistic Quantum Chemistry: The Fundamental Theory of Molecular Science* (John Wiley & Sons, 2014), pp. 654–656.